Journal of Statistical Physics, Vol. 35, Nos. 5/6, 1984

Bifurcation Phenomena near Homoclinic Systems: A Two-Parameter Analysis

P. Gaspard,[1] R. Kapral,[1,2] and G. Nicolis[1]

Received November 15, 1983

The bifurcations of periodic orbits in a class of autonomous three-variable, nonlinear-differential-equation systems possessing a homoclinic orbit associated with a saddle focus with eigenvalues $(\rho \pm i\omega, \lambda)$, where $|\rho/\lambda| < 1$ (Sil'nikov's condition), are studied in a two-parameter space. The perturbed homoclinic systems undergo a countable set of tangent bifurcations followed by period-doubling bifurcations leading to periodic orbits which may be attractors if $|\rho/\lambda| < 1/2$. The accumulation rate of the critical parameter values at the homoclinic system is $\exp(-2\pi|\rho/\omega|)$. A global mechanism for the onset of homoclinicity in strongly contractive flows is analyzed. Cusp bifurcations with bistability and hysteresis phenomena exist locally near the onset of homoclinicity. A countable set of these cusp bifurcations with scaling properties related to the eigenvalues $\rho \pm i\omega$ of the stationary state are shown to occur in infinitely contractive flows. In the two-parameter space, the periodic orbit attractor domain exhibits a spiral structure globally, around the set of homoclinic systems, in which all the different periodic orbits are continuously connected.

KEY WORDS: Bifurcation theory; homoclinic orbit; periodic attractor; chaotic dynamics; bistability; hysteresis; scaling.

1. INTRODUCTION

Nonlinear systems driven far from equilibrium can exhibit a rich variety of transitions to periodic, multiperiodic, or nonperiodic regimes. The modeling

[1] Faculté des Sciences, Université Libre de Bruxelles, Campus Plaine, C. P. 231, 1050 Bruxelles, Belgium.

[2] Permanent address: Department of Chemistry, University of Toronto, Toronto, Ontario M5S 1A1, Canada.

0022-4715/84/0600-0697$03.50/0

of these phenomena at the macroscopic level is usually based on a set of equations describing a continuous time flow, such as the Navier–Stokes or Boussinesq equations of hydrodynamics and the mass-balance equations of chemical kinetics. While considerable progress has been achieved in the perturbative treatment of these equations in the vicinity of simple or degenerate bifurcation points,[1] their global features remain poorly known. In fact, much of our knowledge in this latter direction concerns discrete time mappings.[2,3] These dynamical systems are connected to the underlying continuous time flow through the Poincaré surface of section. However, if one or several stationary states are embedded in the attracting part of the flow, the motion in the phase space is locally distorted so that the bifurcation analysis of the trajectories requires a decomposition of the flow in several successive mappings.

This situation occurs in *homoclinic systems* which may play an important role in determining the global properties of continuous time flows as pointed out recently by some authors.[4–8] *A homoclinic orbit* is a structurally unstable trajectory which is doubly asymptotic to a fixed point of the saddle type as $t \to +\infty$ and $-\infty$.[9]

The importance of such orbits is brought out by the following unexpected result due to Sil'nikov.[10]

Consider the three-variable system

$$\begin{aligned} \dot{x} &= \rho_\mu x - \omega_\mu y + P_\mu(x, y, z) \\ \dot{y} &= \omega_\mu x + \rho_\mu y + Q_\mu(x, y, z) \\ \dot{z} &= \lambda_\mu z + R_\mu(x, y, z) \end{aligned} \tag{1.1}$$

where μ is a parameter, and the functions P_μ, Q_μ, R_μ are analytic in x, y, z, μ vanishing with their first derivatives at the origin $(0,0,0)$. We suppose that the origin behaves as a saddle focus and that there exists for $\mu = 0$ a homoclinic orbit Γ_0 biasymptotic to the origin. Then, if $\nu_0 = |\rho_0/\lambda_0| < 1$:

(i) For $\mu \neq 0$, there exist periodic trajectories in the flow whose number grows unboundedly as $\mu \to 0$.

(ii) For $\mu = 0$, the flow contains in a neighborhood of Γ_0 a subset of trajectories which display random behavior, in the sense that they are in one-to-one correspondence with a shift automorphism with an infinite number of symbols.

On the other hand, for 2-variable homoclinic systems and for the other types of saddle points, in particular if $|\rho_0/\lambda_0| > 1$, the homoclinic orbit generates a single limit cycle when $\mu \neq 0$.[9,10]

The relation between homoclinic trajectories and complex nonperiodic behavior of the chaotic type has been explored for a number of model

systems such as the Lorenz or Rössler models.[5–8,11] In particular, Gaspard and Nicolis[6–8] showed numerically that the onset of homoclinicity in Rössler's model is reflected by several qualitative changes of nearby non-periodic motions: transition from "spiral"- to "screw"-type chaos displaying stronger mixing properties, or appearance of increasing number of oscillatory spikes between intermittent bursts. The transition to screw-type chaos is accompanied by a transition in the next-amplitude map obtained from Poincaré surface of section transverse to the two-dimensional unstable manifold of the flow from a bell-shaped curve to a curve displaying an additional ascending branch. Such double extremum maps have been studied systematically by Fraser and Kapral[12] and shown to give rise to cusp bifurcations with bistability and hysteresis of periodic orbits. An example of this behavior is again provided by the Rössler flow.

The principal goal of the present work is to sharpen the connection between these phenomena and the existence of homoclinic orbits in the system. Furthermore our study completes the above-mentioned Sil'nikov's result, providing information on the possible (periodic) *attractors* existing near this class of homoclinic systems.

In Section 2 we consider a general three-variable system possessing a homoclinic orbit of the Sil'nikov type. We emphasize that the existence of such an orbit allows one to construct a two-dimensional map which captures the properties of the flow near the homoclinic orbit and the associated saddle, and we display this map explicitly.

Section 3 is devoted to the bifurcation analysis of the periodic orbits in the perturbed Sil'nikov homoclinic systems using the above-mentioned two-dimensional map. A general method is proposed which allows one to discuss the various types of bifurcations existing locally in a two-parameter space. We construct the bifurcation loci of these orbits and determine the conditions under which the (tangent) bifurcation may lead to attracting behavior. A rather remarkable feature is that the periodic orbits are generated in pairs for parameter values accumulating at $\mu = 0$ with a rate which depends solely on the linear stability properties of the flow near the saddle. A similar result has been reported quite recently by Glendinning and Sparrow,[13] whose preprint came to our attention when this work was completed.

In Section 4 we study the consequences of the folding of the unstable manifold, observed repeatedly in model systems,[6,8] on the structure of the bifurcation diagram. We model the folding by considering a map in which the quadratic part is dominant and show that the periodic attractors may undergo a countable set of cusp bifurcations with bistability and hysteresis. Attention is focused on the limiting case in which the contraction of the flow along the stable manifold is much greater than the expansion along

the unstable manifold. This case is further analyzed in Section 5 with one-dimensional-map models of the flow. We show that these systems display the main bifurcations found in Section 4 and, in addition, they suggest some further interesting properties of the underlying flow.

The main conclusions are drawn in Section 6, where an attempt is also made to relate the results with some experimental data on the Belousov–Zhabotinski chemical reaction.

2. REDUCTION TO A TWO-DIMENSIONAL MAP

One of the characteristic properties of a homoclinic orbit is its structural instability: the orbit is the intersection of stable and unstable manifolds of the saddle focus and in the generic case these two manifolds no longer intersect if the flow is perturbed. Nevertheless, for parameter values near those characterizing the homoclinic situation a general pattern of reinjection of trajectories near the saddle focus should subsist. In this section we show how this property allows one to construct a two-dimensional map capturing the essential features of the flow.

We consider a general system described by the set of autonomous differential equations (1.1), with μ now understood to be a set of n parameters, $\mu = (\mu_1, \mu_2, \ldots, \mu_n)$, and suppose that when $\mu = 0$ a homoclinic orbit is contained in the flow and that Sil'nikov's condition $\nu_0 = |\rho_0/\lambda_0| < 1$ applies. For definiteness we further require that $\lambda_0 < 0 < \rho_0$, but equivalent results for the opposite inequality can be established by considering the time-reversed flow.

The flows with a homoclinic orbit form a codimension one subset in the set of all the analytic vector fields (1.1). So in the n-dimensional parameter space, the homoclinic systems lie on an $(n-1)$-dimensional hypersurface containing the point $\mu = 0$. We assume that the parametric family of systems (1.1) is transverse to the codimension one set of homoclinic systems.

The analysis of the flow is accomplished through the study of a two-dimensional mapping directly constructed from the flow in the vicinity of the saddle focus. To this end we assume that it is possible to carry out a (C^3) coordinate transformation[3] which linearizes Eqs. (1.1) near the saddle focus 0: in a neighborhood V of 0 Eqs. (1.1) in new coordinates take the

[3] The existence of such a transformation follows from a theorem of Hartman[14] provided the eigenvalues do not form any low-order resonances. While the results obtained here are independent of the resonance condition on the eigenvalues, this requirement facilitates calculations.

form

$$\begin{aligned} \dot{x} &= \rho_\mu x - \omega_\mu y \\ \dot{y} &= \omega_\mu x + \rho_\mu y \\ \dot{z} &= \lambda_\mu z \end{aligned} \tag{2.1}$$

We have also denoted the new coordinates (x, y, z) since the old coordinates will not enter in the sequel. The geometrical features of the flow which are relevant for the construction of the mapping are sketched in Fig. 1. The unstable manifold W_u of the saddle focus is the plane $z = 0$, while the stable manifold W_s is the line $x = y = 0$. We imagine that 0 is enclosed by a cylinder which is defined by $0 < r < R$ and $-Z < z < Z$ in the cylindrical coordinates $x = r\cos\varphi$, $y = r\sin\varphi$ and $z = z$.

Two successive maps of the flow may now be constructed: (1) the map T_0 induced by the flow within the cylinder in the vicinity of the saddle focus, which maps points from the upper disk Σ_1 of the cylinder to its lateral surface Σ_0; and (2) the map T_1 constructed from the global part of

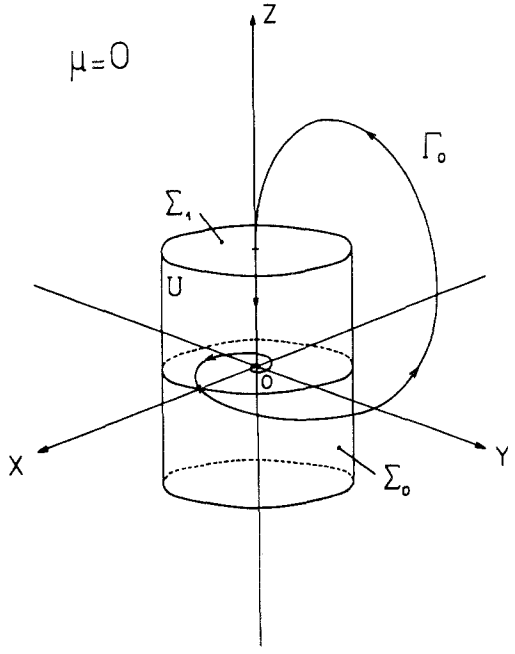

Fig. 1. Schematic phase portrait of the saddle focus 0, the cylinder U, and the homoclinic orbit Γ_0 existing when $\mu = 0$ (see text).

the flow near $\mu = 0$, which maps points from Σ_0 to Σ_1. The equations for Σ_1 and Σ_0 are, respectively,

$$\begin{aligned} &\Sigma_1: \quad z_1 = Z, \qquad 0 < r_1 < R \\ &\Sigma_0: \quad r_0 = R, \qquad -\pi \leqslant \varphi_0 < \pi \end{aligned} \tag{2.2}$$

The φ coordinate is chosen so that the homoclinic orbit Γ_0 crosses Σ_0 at $\varphi_0 = 0$, $z_0 = 0$. (Points on the two surfaces will be labeled with the appropriate subscript.) The map $T_0: (x_1, y_1) \to (\tilde{\varphi}_0, \tilde{z}_0)$ follows from direct integration of Eqs. (2.1):

$$T_0: \begin{cases} x_1 = R\left(\dfrac{\tilde{z}_0}{Z}\right)^{\nu} \cos\left(\tilde{\varphi}_0 + \dfrac{\omega}{|\lambda|} \log \dfrac{\tilde{z}_0}{Z}\right) \equiv F(\tilde{\varphi}_0, \tilde{z}_0) \\ y_1 = R\left(\dfrac{\tilde{z}_0}{Z}\right)^{\nu} \sin\left(\tilde{\varphi}_0 + \dfrac{\omega}{|\lambda|} \log \dfrac{\tilde{z}_0}{Z}\right) \equiv G(\tilde{\varphi}_0, \tilde{z}_0) \end{cases} \tag{2.3}$$

with $\nu = |\rho/\lambda|$. We hereafter choose ω to be positive. The transit time of the trajectory in the cylinder is given by $\tilde{t} = (1/|\lambda|)\log(Z/\tilde{z}_0)$.

Here and below we no longer consider the eigenvalues as functions of the μ parameters but as parameters themselves, i.e., the parameters of the class of systems studied are now $(\rho, \omega, \lambda, \mu_1, \ldots, \mu_n)$. The bifurcations of the original parametric family (1.1) will be obtained thereafter because the set $(\rho_\mu, \omega_\mu, \lambda_\mu)$ is embedded in the (ρ, ω, λ)-parameter subspace.

Owing to the existence of a homoclinic orbit when $\mu = 0$, the flow outside the cylinder maps Σ_0 onto Σ_1,

$$T_1: \begin{cases} x_1 = L_\mu(\varphi_0, z_0) \\ y_1 = M_\mu(\varphi_0, z_0) \end{cases} \tag{2.4}$$

with $L_0(0,0) = M_0(0,0) = 0$, which is simply the condition for the existence of a homoclinic orbit in our construction: ($\varphi_0 = 0$, $z_0 = 0$) on W_μ is mapped into ($x_1 = 0$, $y_1 = 0$) on W_s. In view of this latter condition and the assumed C^3 character of the linearizing transformation we may write the T_1 map as

$$T_1: \begin{cases} x_1 = A + a_1\varphi_0 + a_2 z_0 + a_{11}\varphi_0^2 + 2a_{12}\varphi_0 z_0 + a_{22} z_0^2 + O(\varphi_0^p z_0^q) \\ \quad \equiv A + \mathscr{A}(\varphi_0) + O(z_0) \\ y_1 = B + b_1\varphi_0 + b_2 z_0 + b_{11}\varphi_0^2 + 2b_{12}\varphi_0 z_0 + b_{22} z_0^2 + O(\varphi_0^p z_0^q) \\ \quad \equiv B + \mathscr{B}(\varphi_0) + O(z_0) \end{cases} \tag{2.5}$$

with $A = B = 0$ when $\mu = 0$ ($p + q \geqslant 3$). Note that the T_1 map preserves the orientation of the phase space so that its Jacobian (cf. Section 3.1) is positive. The bifurcation analysis will be made in the parameter space of

the coefficients of the partial Taylor expansion (2.5). The bifurcations for a parametric family of systems (1.1) could thereafter be deduced from this study since such a family is embedded in the set of systems (2.5). In Eqs. (2.5), we have isolated A and B as the important bifurcation parameters because they vanish when $\mu = 0$; we shall confine our attention subsequently to the (A, B)-parameter space.

Given the structure of the T_1 map in Eqs. (2.5) we may immediately deduce the locus of homoclinic systems in the (A, B) plane. A homoclinic orbit exists in the flow whenever W_u and W_s intersect. Since $z_0 = 0$ is the equation of $W_u \cap \Sigma_0$, the curve $W_u \cap \Sigma_1$ is the mapping of $z_0 = 0$ by T_1, i.e.,

$$W_u \cap \Sigma_1 : \quad \begin{cases} x_1 = A + \mathscr{A}(\varphi_0) \\ y_1 = B + \mathscr{B}(\varphi_0) \end{cases} \tag{2.6}$$

But $(x_1 = 0, y_1 = 0)$ is the equation defining $W_s \cap \Sigma_1$, so the flow contains a homoclinic orbit if a φ_0 exists such that

$$H: \quad \begin{cases} A = -\mathscr{A}(\varphi_0) \\ B = -\mathscr{B}(\varphi_0) \end{cases} \tag{2.7}$$

These equations specify a mapping of the point φ_0 of $W_u \cap \Sigma_0$ onto the

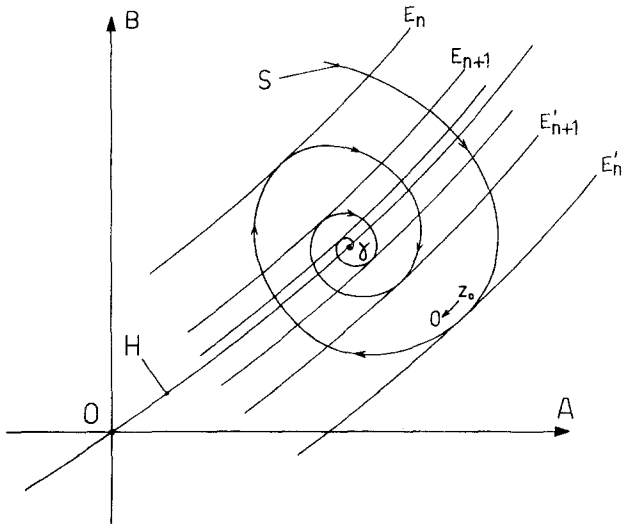

Fig. 2. Schematic diagram of the (A, B) parameter space. H is the set of homoclinic systems (2.7). S is a spiral for φ_0 fixed and $z_0 \to 0$ of the family (3.1). γ is the center (2.7) of the spiral S. E_k and E'_k are curves of the envelope of family (3.1).

(A, B)-parameter plane and demonstrate that the homoclinic systems lie on the line H (see Fig. 2) in this plane (so that the homoclinic systems form a codimension one subset).

The flow maps a domain of Σ_0 onto Σ_0 by the combined map $T = T_0 T_1 : (\varphi_0, z_0) \to (\tilde{\varphi}_0, \tilde{z}_0)$. We remark that, as a consequence of the assumed regularity of Eqs. (1.1) and that of the linearizing transformation, the functions L_μ and M_μ determining the T_1 map exist in a neighborhood σ_0 of $\varphi_0 = z_0 = 0$ on Σ_0 defined by

$$\sigma_0 : \quad -\eta < \varphi_0 < \eta, \qquad -\zeta < z_0 < \zeta \tag{2.8}$$

with $\eta < \pi$ and $\zeta < Z$. All of the results subsequently deduced from the study of the map T concern flow trajectories crossing Σ_0 in the domain σ_0. In the next section the periodic trajectories of the flow are studied through the above-defined map.

3. BIFURCATION ANALYSIS OF THE PERIODIC ORBITS

Consider a periodic orbit going through the point (φ_0, z_0) of Σ_0 which is a fixed point of the map T, so that $(\varphi_0, z_0) = (\tilde{\varphi}_0, \tilde{z}_0)$. The question is: What is the (A, B) flow that contains this orbit? Using Eqs. (2.3) and (2.5) we may write for such an orbit

$$P: \begin{cases} A = R\left(\dfrac{z_0}{Z}\right)^{\nu} \cos\left(\varphi_0 + \dfrac{\omega}{|\lambda|} \log \dfrac{z_0}{Z}\right) - \mathscr{A}(\varphi_0) - O(z_0) \\ B = R\left(\dfrac{z_0}{Z}\right)^{\nu} \sin\left(\varphi_0 + \dfrac{\omega}{|\lambda|} \log \dfrac{z_0}{Z}\right) - \mathscr{B}(\varphi_0) - O(z_0) \end{cases} \tag{3.1}$$

These equations define a mapping P from this set of periodic orbits in the phase space onto the parameter plane. Since we consider flows in which Sil'nikov's condition $\nu < 1$ is satisfied the terms $O(z_0^{\nu})$ dominate in the limit $z_0 \to 0$. For φ_0 constant in such a limit Eqs. (3.1) generate a logarithmic spiral in the (A, B) plane whose center $\gamma = (-\mathscr{A}(\varphi_0), -\mathscr{B}(\varphi_0))$ lies on the line H of homoclinic systems (Fig. 2). The spiral is parameterized by φ_0 and if φ_0 varies the center of the spiral moves along H while the entire spiral rotates. This family of spirals is the representation in the (A, B) plane of the set of all the flows containing periodic orbits of the once-iterated T map.

The P mapping is not one-to-one but several-to-one. The number of (φ_0, z_0) points in the phase space mapped by P on an (A, B) point corresponds to the number of periodic orbits in the (A, B) flow. The locus of points in the (A, B) plane where this number changes corresponds to the locus where a bifurcation occurs in the flow. Thus, to study the bifurcations

of the periodic trajectories, we must consider the singularities of the P mapping and the stability of the periodic orbits near these singularities.

As P is a mapping from a plane onto a plane, according to the general theory of such mappings,[15] there exist two types of structurally stable singularities: (1) folds which are curves and (2) cusps, which are isolated points on the fold curves.

In the following sections, we present a discussion of the bifurcations of periodic orbits occurring near these singularities of the P mapping and a study of their stability.

3.1. Tangent Bifurcation

The fold lines are the envelopes of the family of spirals (they are schematically depicted in Fig. 2). It is clear that a fold cannot exist at points where the Jacobian determinant of P is different from zero since there the P map is invertible. In other words the fold loci are the roots of[15]

$$J = \partial_{z_0} A \partial_{\varphi_0} B - \partial_{\varphi_0} A \partial_{z_0} B = 0 \tag{3.2}$$

By a straightforward calculation one may demonstrate that one of the eigenvalues of the linearized T map is $\Lambda = +1$ on the fold line, thus, this line can be identified as the line of tangent bifurcations (tangent boundary) in the (A, B) plane. Using Eqs. (2.3) and (2.4) for the T_0 and T_1 maps, respectively, the linearized T map reads

$$\begin{bmatrix} \delta\tilde{z}_0 \\ \delta\tilde{\varphi}_0 \end{bmatrix} = Q_0^{-1} \begin{bmatrix} \partial_{\varphi_0} G & -\partial_{\varphi_0} F \\ -\partial_{z_0} G & \partial_{z_0} F \end{bmatrix} \begin{bmatrix} \partial_{z_0} L & \partial_{\varphi_0} L \\ \partial_{z_0} M & \partial_{\varphi_0} M \end{bmatrix} \begin{bmatrix} \delta z_0 \\ \delta\varphi_0 \end{bmatrix} \tag{3.3}$$

whose characteristic equation multiplied by Q_0 is

$$\begin{aligned} &\Lambda^2 (\partial_{z_0} F \partial_{\varphi_0} G - \partial_{\varphi_0} F \partial_{z_0} G) \\ &\quad - \Lambda (\partial_{z_0} F \partial_{\varphi_0} M + \partial_{\varphi_0} G \partial_{z_0} L - \partial_{\varphi_0} F \partial_{z_0} M - \partial_{z_0} G \partial_{\varphi_0} L) \\ &\quad + (\partial_{z_0} L \partial_{\varphi_0} M - \partial_{\varphi_0} L \partial_{z_0} M) = 0 \end{aligned} \tag{3.4}$$

or

$$\Lambda^2 - C\Lambda + D = 0$$

Here $Q_0 = \partial_{z_0} F \partial_{\varphi_0} G - \partial_{\varphi_0} F \partial_{z_0} G$ is the Jacobian of the T_0 map. If $\Lambda = +1$ is substituted into this characteristic equation the envelope equation $J = 0$ is recovered.

We next study the structure and character of the fold or tangent bifurcation lines. Direct calculation of the Jacobian determinant leads to

the following envelope or tangent boundary equation:

$$\left[\mathscr{A}'(\varphi_0)^2 + \mathscr{B}'(\varphi_0)^2\right]^{1/2}\cos\left[\varphi_0 + \frac{\omega}{|\lambda|}\log\frac{z_0^*}{Z} + \arctan\frac{\omega}{\rho} + \arctan\frac{\mathscr{A}'(\varphi_0)}{\mathscr{B}'(\varphi_0)}\right]$$

$$= \frac{R\rho}{(\rho^2+\omega^2)^{1/2}}\left(\frac{z_0^*}{Z}\right)^{\nu} + O(z_0^{*1-\nu}) \tag{3.5}$$

When $z_0^* \to 0$ the right-hand side of Eq. (3.5) vanishes and provided $\mathscr{A}'(\varphi_0)^2 + \mathscr{B}'(\varphi_0)^2 \neq 0$ for φ_0 near zero the solutions for the fold loci are the roots of the cosine function:

$$z_0^*(\varphi_0) = Z\exp\left\{-\frac{|\lambda|}{\omega}\left[2\pi n + \begin{pmatrix}\pi/2\\ 3\pi/2\end{pmatrix} + \varphi_0 + \arctan\frac{\omega}{\rho} + \arctan\frac{\mathscr{A}'(\varphi_0)}{\mathscr{B}'(\varphi_0)} + \Delta\Psi^*\right]\right\} \tag{3.6}$$

where $\Delta\Psi^* = O(z_0^{*\nu}) + O(z_0^{*1-\nu})$ and n is large enough. Thus there exist two countable sets of fold loci. We may find the tangent boundaries in the (A, B) plane by simply substituting Eq. (3.6) into the P map, Eqs. (3.1):

$$A^* = -\mathscr{A}(\varphi_0) \mp RU(\varphi_0)\exp\left\{-\frac{\rho}{\omega}\left[2\pi n + \begin{pmatrix}\pi/2\\ 3\pi/2\end{pmatrix}\right]\right\} + O(e^{-4\pi n\rho/\omega})$$

$$+ O(e^{-2\pi n(|\lambda|/\omega)})$$

$$B^* = -\mathscr{B}(\varphi_0) \pm RV(\varphi_0)\exp\left\{-\frac{\rho}{\omega}\left[2\pi n + \begin{pmatrix}\pi/2\\ 3\pi/2\end{pmatrix}\right]\right\} + O(e^{-4\pi n\rho/\omega}) \tag{3.7}$$

$$+ O(e^{-2\pi n(|\lambda|/\omega)})$$

We shall not write the explicit forms of the functions $U(\varphi_0)$ and $V(\varphi_0)$ since their detailed structure is not important for the discussion that follows. (They are not simultaneously vanishing when $\varphi_0 = 0$.) Equation (3.7) shows that on both sides of the line of homoclinic systems H there is a family of tangent bifurcation lines accumulating at H with a geometric rate.

More specifically, from Eqs. (3.7), the critical parameter values $\mu_n^{t\pm}$ for a one-parameter family of systems (1.1) transverse to the codimension one set H of the homoclinic systems satisfy

$$\lim_{n\to\infty}\frac{\mu_{n+1}^{t\pm} - \mu_n^{t\pm}}{\mu_n^{t\pm} - \mu_{n-1}^{t\pm}} = \exp(-2\pi|\rho_0/\omega_0|) \tag{3.8}$$

where the $\pm$ superscript refers to the fact that two such sequences appear on either side of H and $\rho_0 \pm i\omega_0$ are the complex conjugate eigenvalues at parameter value $\mu = 0$.

Equation (3.8) expresses the interesting result that the accumulation rate of these tangent bifurcation loci is determined solely by the ρ and ω parameters characterizing the flow winding motion about the saddle focus. We shall comment in more detail about this result in the subsequent sections, but first we study the stability of the solutions produced by the tangent process.

The stability of the solutions can be determined by referring to the characteristic equation (3.4). We noted that on a fold line one eigenvalue is $\Lambda_+^* = +1$ and, thus, denoting the values of C and D on this line by C^* and D^*, respectively, we obtain from Eq. (3.4) that $C^* = 1 + D^*$. With this condition the other eigenvalue of Eq. (3.4) is

$$\Lambda_-^* = D^* = \frac{Q_1}{Q_0} = \frac{\partial_{z_0} L \partial_{\varphi_0} M - \partial_{\varphi_0} L \partial_{z_0} M}{(R^2 \nu / Z)(z_0^*/Z)^{2\nu - 1}} \tag{3.9}$$

which shows that Λ_-^* is the ratio of the Jacobian determinant of the T_1 map, Q_1, to that of the T_0 map, Q_0. The results of the explicit calculation of these quantities is given in the last part of Eq. (3.9).

If the fold line is traversed, the periodic orbit goes through a point $(z_0^*(\varphi_0) + \Delta z_0, \varphi_0)$ in a neighborhood of the fold point $(z_0^*(\varphi_0), \varphi_0)$. Setting

$$C = 1 + D^* + \epsilon_1, \qquad D = D^* + \epsilon_2$$

We find that the eigenvalues of the characteristic equation are now given by

$$\begin{aligned} \Lambda_+ &= 1 + \frac{\epsilon_1 - \epsilon_2}{1 - D^*} + O(\epsilon^2) \\ \Lambda_- &= D^*(1 + O(\epsilon)) \end{aligned} \tag{3.10}$$

with

$$\begin{gathered} \epsilon = (\epsilon_1^2 + \epsilon_2^2)^{1/2} \quad \text{and} \\ \epsilon_1 - \epsilon_2 = \Delta z_0 \times (\text{a nonvanishing function of } \varphi_0 \text{ and } z_0^*) \end{gathered} \tag{3.11}$$

It follows that the correction to the critical eigenvalue Λ_+ is proportional to Δz_0 and can therefore have both positive and negative values around the fold loci.

From this fact and Eq. (3.9) we may deduce the following results. If $Q_1 \neq 0$ [note: $Q_1 \neq 0$ implies that $\mathscr{A}'(\varphi_0)^2 + \mathscr{B}'(\varphi_0)^2 \neq 0$ which was assumed earlier], then (1) for $\nu < 1/2$, $D^* \to 0$ as $z_0^* \to 0$ and a pair of stable node-saddle periodic orbits is generated at the tangent bifurcation, and (2)

for $1/2 < \nu < 1$, $D^* \to \infty$ as $z_0^* \to 0$ and a pair of unstable node-saddle orbits is generated.

Having established the locus and character of the tangent bifurcation process we turn to the calculation of the domains within which the periodic orbits produced by this process exist.

3.2. Period-Doubling Bifurcation

The periodic orbits born at the fold line by a tangent bifurcation undergo a period-doubling (subharmonic) bifurcation when one eigenvalue of the T map is $\Lambda = -1$. The locus of such bifurcations can be computed from the characteristic equation (3.4) with $\Lambda = -1$. Denoting the value of z_0 at such loci by z_0^{**} we find

$$\left[\mathscr{A}'(\varphi_0)^2 + \mathscr{B}'(\varphi_0)^2\right]^{1/2} \times \cos\left[\varphi_0 + \frac{\omega}{|\lambda|}\log\frac{z_0^{**}}{Z} + \arctan\frac{\omega}{\rho} + \arctan\frac{\mathscr{A}'(\varphi_0)}{\mathscr{B}'(\varphi_0)}\right] = -\frac{R\rho}{(\rho^2+\omega^2)^{1/2}}\left(\frac{z_0^{**}}{Z}\right)^{\nu} + O(z_0^{**1-\nu}) \tag{3.12}$$

This equation should be compared with the analogous equation for the tangent boundary [Eq. (3.5)]. Assuming again that $\mathscr{A}'^2 + \mathscr{B}'^2 \neq 0$, the solutions of this equation are in first approximation the same as those of Eq. (3.5); the difference between them appears in the second approximation:

$$z_0^*(\varphi_0) - z_0^{**}(\varphi_0) = e^{-2\pi n(|\lambda|/\omega)}\left[O(e^{-2\pi n(\rho/\omega)}) + O(e^{-2\pi n[(|\lambda|-\rho)/\omega]})\right] \tag{3.13}$$

As in the earlier calculation for the tangent bifurcation, this result may be substituted into the P map to obtain the loci of such bifurcations in the (A,B) plane. Letting $\mu^{h\pm}$ signify the critical parameter values where subharmonic bifurcations occur for a one-parameter family of systems (1.1) transverse to the codimension one subset H of homoclinic systems we may now state the following:

(1) If $\nu < 1/2$, the stable node of the stable node-saddle pair of the T map becomes a saddle at the harmonic boundary. The first term on the right side of Eq. (3.13) is dominant in this case and the stability window of the stable node is

$$\mu_n^{t\pm} - \mu_n^{h\pm} = O(e^{-4\pi n(\rho_0/\omega_0)}) \tag{3.14}$$

(2) If $1/2 < \nu < 1$, the unstable node of the unstable node-saddle pair of the T map becomes a saddle at the harmonic boundary. In this case the second term on the right side of Eq. (3.13) is dominant and

$$\mu_n^{t\pm} - \mu_n^{h\pm} = O(e^{-2\pi n(|\lambda_0|/\omega_0)}) \tag{3.15}$$

where $(\rho_0 \pm i\,\omega_0, \lambda_0)$ are the eigenvalues of the saddle fixed point for the parameter value $\mu = 0$.

The results of this section for the important case of $\nu < 1/2$ are displayed in the schematic bifurcation diagram in (z_0, μ) plane of Fig. 3. The figure shows how the various solutions are connected across the $\mu = 0$ line. The supercritical period-doubling bifurcations indicated in the figure are suggested by one-dimensional-map models like the one discussed in Section 5. A full study of such bifurcations entails a study of the periodic orbits of higher powers of the T map. Although we do not study these bifurcations here we shall comment on some of their features in Sections 4 and 5.

In addition to the bifurcation of periodic orbits studied here, there also exist bifurcations generating a countable set of additional homoclinic flows as shown in Refs. 6 and 7, which all occur on a single side of the hypersurface H of homoclinic systems (the side $\mu > 0$ in Fig. 3 because, as pointed out in Section 2, the T_1 map preserves the orientation of the phase space). The bifurcation analysis carried out here applies to each of these

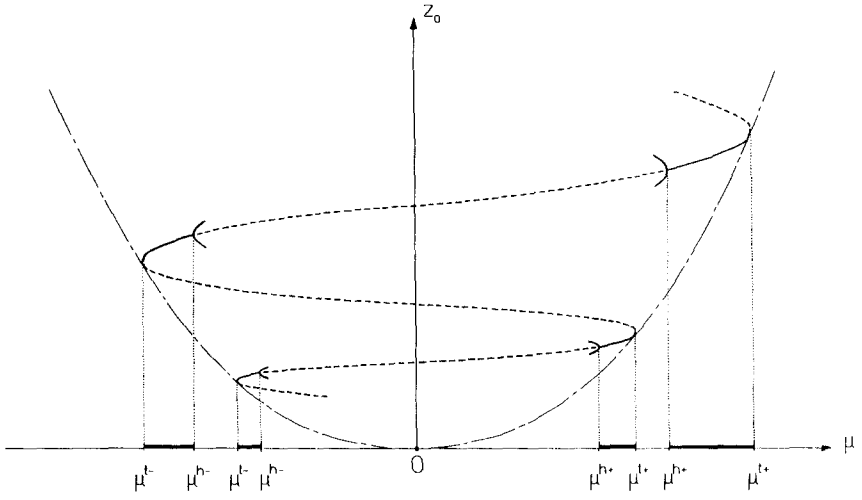

Fig. 3. Bifurcation diagram of periodic orbits near homoclinic systems in the case $|\rho_0/\lambda_0| < 1/2$.

homoclinic flows so that, besides the sequence of tangent bifurcations associated with the original homoclinic flow depicted in Fig. 3, there exist such sequences satisfying the accumulation rate (3.8), associated to *each* of these homoclinic flows. In the case $0 < \nu < 1/2$, this result shows the complexity of the bifurcations of the periodic attractors near Sil'nikov's homoclinic systems and suggests that the coexistence of several attractors in a given flow near these systems is a possibility.

3.3. Cusp Bifurcation

Besides the fold singular points, the P mapping may also contain cusp singular points (as mentioned at the beginning of Section 3), which are isolated points on the folds: they are the turning points of the envelope curve. At a cusp point a bifurcation occurs with birth of two new solutions in addition to an old one. If the periodic orbit existing outside the cusp is stable, then bistability arises within the cusp and is associated with hysteresis.

A point p is a cusp point if the following three conditions are satisfied:[15]

$$J(p) = 0 \tag{3.16}$$

$$(V \cdot D)P(p) = 0 \tag{3.17}$$

$$(V \cdot D)(V \cdot D)P(p) \neq 0 \tag{3.18}$$

where $(V \cdot D)$ is the derivative in the direction of V, which is the vector tangent to the fold curve in the (φ_0, z_0) plane

$$V = (-\partial_{\varphi_0} J, \partial_{z_0} J) \tag{3.19}$$

Thus a cusp point is an isolated point on a fold which is solution of the two following equations with two unknown variables

$$J = 0 \tag{3.16'}$$

$$K_1 = \partial_{z_0} A \partial_{\varphi_0} J - \partial_{\varphi_0} A \partial_{z_0} J = 0 \tag{3.20}$$

In the following section, we will show that cusp points may exist in the P mapping besides fold points near homoclinic systems for which the quadratic terms of the T_1 map are dominant [see Eqs. (2.5)].

In this section we have intentionally presented the results in a rather general form in order to describe the gross features of the bifurcation structure near homoclinic systems. We have also focused on the case where the Jacobian of the T_1 map, Q_1, is nonzero for φ_0 near zero. In the

following section we give detailed analysis of a specific model of the T_1 map for a strongly contractive system where $Q_1 = 0$.

4. QUADRATIC MODEL

A common mechanism for the appearance of a homoclinic orbit in a very contractive flow involves the folding of the unstable manifold by the global part of the flow followed by its reinjection in the vicinity of the saddle focus. This mechanism exists for a number of differential-equation systems; in particular, in a Rössler model,[16] which we use to illustrate some of the phenomena described in this paper.

A model of a flow where such a mechanism operates is studied with the aid of a global T_1 map whose quadratic part is dominant. Recall that our previous discussion concerned a T_1 map with a dominant linear part. The full analysis of the quadratic model reveals the existence of a countable set of cusp bifurcations associated with hysteresis and bistability in the flow. Our study indicates that these phenomena are expected in the vicinity of homoclinic systems. The utility of the two-parameter study of bifurcation processes given in the preceding section is clearly demonstrated for these folding flows: the cusp bistabilities are fully revealed only in the two-parameter plane.

The global T_1 map for the quadratic model is obtained from Eqs. (2.5) by limiting the functions $\mathscr{A}(\varphi_0)$ and $\mathscr{B}(\varphi_0)$ to quadratic nonlinearities. We select the form

$$T_1: \quad \begin{cases} x_1 = \epsilon - \eta\varphi_0 \\ y_1 = -\delta + c\varphi_0^2 + dz_0 \end{cases} \tag{4.1}$$

with the parameters η, d (and c) chosen positive so that T_1 conserves the orientation in the three-dimensional phase space. The φ_0^2 part of T_1 gives rise to the folding process, while ϵ and δ model the manner in which the flow is reinjected near the unstable fixed point. Clearly the (A, B)-parameter space is the (ϵ, δ) plane for this model. From Eqs. (2.7) and (4.1) the set of homoclinic systems in this plane is the parabola $\delta = c(\epsilon/\eta)^2$. If $\eta = 0$ homoclinic systems exist in the half line $\epsilon = 0$, $\delta \geqslant 0$. Since the Jacobian of the T_1 map is $Q_1 = \eta d$, the case $\eta = 0$ corresponds to an infinitely contractive global map. This very contractive character is common to many physical systems and responsible for the fact that they admit a description in terms of one-dimensional maps. We confine our discussion to this $\eta = 0$ limit. Since the limit $|\lambda| \gg |\rho|$ a flow near homoclinicity satisfying $\lambda < 0 < \rho$ is strongly contractive, we assume that ν appearing in T_0 satisfies $\nu < 1/2$.

We may now follow the bifurcation analysis of Section 3. The explicit form of the P map is

$$P: \begin{cases} \epsilon = R\left(\frac{z_0}{Z}\right)^{\nu} \cos\left(\varphi_0 + \frac{\omega}{|\lambda|} \log \frac{z_0}{Z}\right) \\ \delta = -R\left(\frac{z_0}{Z}\right)^{\nu} \sin\left(\varphi_0 + \frac{\omega}{|\lambda|} \log \frac{z_0}{Z}\right) + c\varphi_0^2 + dz_0 \end{cases} \tag{4.2}$$

The tangent bifurcation loci are the solutions of

$$J = \partial_{z_0}\epsilon\partial_{\varphi_0}\delta - \partial_{\varphi_0}\epsilon\partial_{z_0}\delta = 0 \quad \text{or}$$

$$2c\varphi_0 \cos\left(\varphi_0 - \alpha^* + \arctan\frac{\omega}{\rho}\right) = \frac{R\rho}{(\rho^2+\omega^2)^{1/2}} e^{-(\rho/\omega)\alpha^*} + O(e^{-(|\lambda|/\omega)\alpha^*}) \tag{4.3}$$

where

$$\alpha^* = -\frac{\omega}{|\lambda|} \log \frac{z_0^*}{Z} \tag{4.4}$$

In the limit $z_0^* \to 0$, $\alpha^* \to \infty$ and the right side of Eq. (4.3) vanishes, yielding two sets of solutions: either

$$\cos\left(\varphi_0 - \alpha^* + \arctan\frac{\omega}{\rho}\right) = 0 \tag{4.5}$$

or

$$\varphi_0 = 0 \tag{4.6}$$

The solutions of Eq. (4.5) have the same character as those analyzed in Section 3, while the new solution is the spiral $\varphi_0 = 0$ [cf. Eqs. (4.2)] in the (ϵ, δ) plane. In Section 3, a solution like Eq. (4.6) was excluded because of the assumption that $\mathscr{A}'(\varphi_0)^2 + \mathscr{B}'(\varphi_0)^2 \neq 0$.

If α^* is finite the solutions of Eq. (4.3) are the intersections of a cosine function and an exponential function whose intersection with the $\alpha^* = 0$ axis is proportional to φ_0^{-1}. For α^* large enough and $\varphi_0 \neq 0$ there always exists a countable set of solutions, which is

$$\begin{aligned} \alpha^* &= 2\pi n + \begin{pmatrix} \pi/2 \\ 3\pi/2 \end{pmatrix} + \varphi_0 + \arctan\frac{\omega}{\rho} + \Delta\Psi^* \\ \Delta\Psi^* &= \mp \frac{R\rho}{2c\varphi_0(\rho^2+\omega^2)^{1/2}} e^{-(\rho/\omega)\alpha^*} + O(e^{-(|\lambda|/\omega)\alpha^*}) \end{aligned} \tag{4.7}$$

provided n is large enough. When $\varphi_0 \to 0$ from positive or negative values these solutions disappear pairwise at points (α^*, φ_0) where the cosine function is tangent to the exponential function. Hence, the asymptotic solutions are connected pairwise when $\varphi_0 \simeq 0$.

Following Section 3 we may also study the harmonic (period-doubling) boundaries for this model. The loci of these boundaries are found from the solutions of

$$2c\varphi_0\cos\left(\varphi_0 - \alpha^{**} + \arctan\frac{\omega}{\rho}\right) = -\frac{R\rho}{(\rho^2+\omega^2)^{1/2}}e^{-(\rho/\omega)\alpha^{**}} + O(e^{-(|\lambda|/\omega)\alpha^{**}}) \tag{4.8}$$

where α^{**} is given by Eq. (4.4) with z_0^* replaced by z_0^{**}. According to the stability analysis in Section 3, since $\nu < 1/2$ pairs of stable node-saddle orbits are born at the tangent boundary with a domain of existence bounded by the line of period-doubling bifurcations.

In order to reveal the full periodic orbit structure we have solved Eqs. (4.3) and (4.8) numerically for the following parameter values: $\rho = 0.2$, $\omega = 1$, $\lambda = -5$, $c = 0.1$, $d = 0.1$, and $R = Z = 1$. We have taken α^* and α^{**} large enough so that the last terms in Eqs. (4.3) and (4.8) can be neglected. The calculation is carried out by selecting a φ_0 and determining α^* or α^{**}; these values are then substituted into the P map to determine the phase diagram in the (ϵ, δ) plane. The results of the calculation are shown in Fig. 4.

The figure displays some interesting geometrical features of the bifurcations. The global structure of the periodic attractor domain is governed by the spiral geometry arising from the saddle-focus character of the stationary state. In addition, it is clear that all the periodic attractors are connected among themselves in the two-parameter space. Thus, with two control parameters the system can be deformed continuously to move from one branch on the spiral to another. An enlargement of one of the regions where the different branches are connected with the spiral domain is shown in Fig. 4b. The cusp structure of inner tangent boundary is clearly evident in this enlargement. This structure is typical of a system exhibiting bistability and hysteresis phenomena.

The locations of the cusp points can be simply computed for this model. They are solutions of the Eqs. (3.16) and (3.20). The cusp points are expected near the connection points between the solutions (4.5) and (4.6) of the envelope. The solutions in the phase space, of the cusp equations satisfying this requirement are

$$z_0 = Z\exp\left\{-\frac{|\lambda|}{\omega}\left[p\pi + \frac{\pi}{2} + \arctan\frac{\omega}{\rho} + O(e^{-(\rho/\omega)(p\pi/3)})\right]\right\} \tag{4.9}$$

$$\varphi_0 = \frac{1}{2c}\left(\frac{2cR^2\rho}{\omega}\right)^{1/3}\left(\frac{z_0}{Z}\right)^{2\nu/3}\left[1 + O(z_0^{\nu/3})\right] \tag{4.10}$$

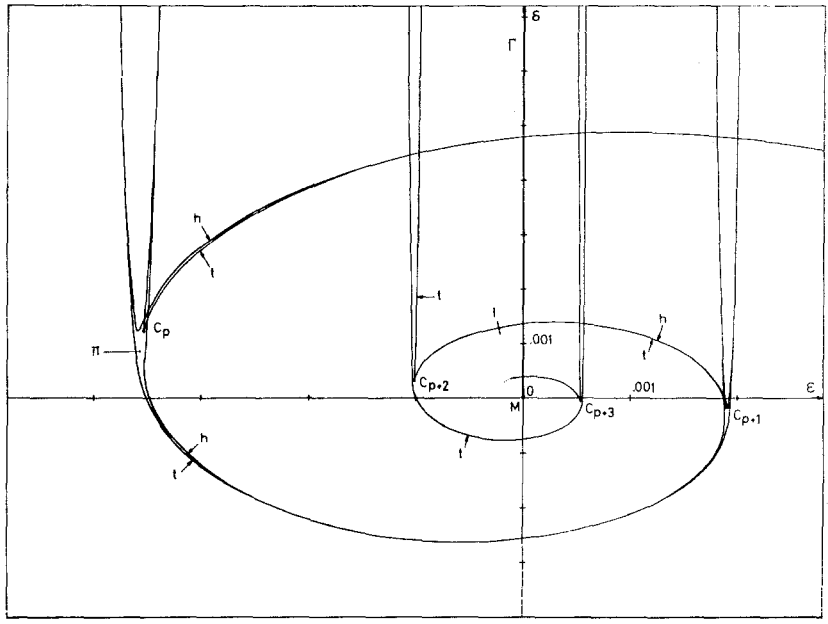
δ
Γ
h
t
C_p
π
t
.001
h
t
C_{p+2}
0
M
C_{p+3}
.001
ε
C_{p+1}
t
h
t

(a)

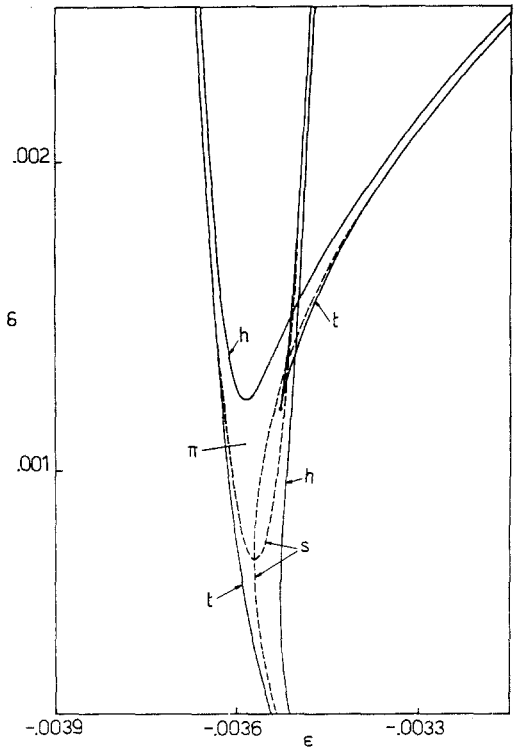
.002
δ
.001
h
t
π
h
s
t
-.0039
-.0036
-.0033
ε

(b)

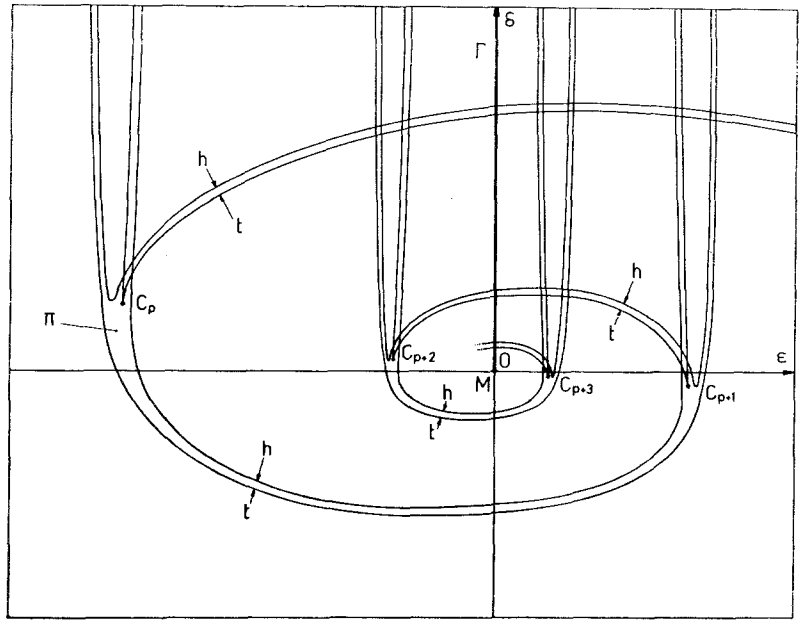

(c)

Fig. 4. (a) Periodic attractor existence domain π in the (ϵ, δ)-parameter space for the quadratic model (4.1). π is contained between the tangent t and the period-doubling h bifurcation loci. The curve Γ is the set of homoclinic systems. M is the end point of the set Γ. $C_p, \ldots, C_{p+3}$ are cusp points. The harmonic boundary is not drawn at the left of line 1. (b) Enlargement of the π domain near the C_p cusp bifurcation. t and h are, respectively, the tangent and the period-doubling boundaries. The broken line s is the set of systems containing a superstable periodic orbit. Bistability and hysteresis occur near the cusp point C_p. (c) Schematic representation of the tangent and harmonic boundaries of the π domain.

where p is a (large enough) integer. In the (ϵ, δ) plane, the cusp points are

$$\begin{cases} \epsilon_p = (-)^{p+1} R \left(\dfrac{z_0}{Z} \right)^{\nu} \dfrac{\omega}{(\rho^2 + \omega^2)^{1/2}} + O(z_0^{4\nu/3}) \\ \delta_p = (-)^{p} R \left(\dfrac{z_0}{Z} \right)^{\nu} \dfrac{\rho}{(\rho^2 + \omega^2)^{1/2}} + O(z_0^{4\nu/3}) \end{cases} \tag{4.11}$$

with z_0 given by (4.9). These solutions satisfy the last condition (3.19) and so the cusp points are nondegenerate. Asymptotically the cusp points are located on the line

$$\omega \delta_p + \rho \epsilon_p = O(z_0^{4\nu/3}) \tag{4.12}$$

$Q_1 = 0$ for the infinitely contractive model studied here and thus $D^* = 0$ [Eq. (3.9)]. Since one of the eigenvalues is always zero the notion of

superstable orbits can be introduced. Such orbits exist when both eigenvalues vanish. The superstable loci can be calculated easily: one of these loci is the spiral $\varphi_0 = 0$ while the others form a countable set and are connected to the spiral as shown by the dashed lines s in Fig. 4b. The notion of superstable orbits is especially useful for studying the above phenomena in one-dimensional-map model. This analysis will be carried out in Section 5 where the nature of the bistabilities mentioned above is discussed in more detail.

The results of this section demonstrate the cusp bistabilities are likely to exist near homoclinic systems involving a global folding of the unstable manifold of the saddle focus. For the infinitely contractive model there exists a countable set of cusp bistabilities in the vicinity of the $\epsilon = \delta = 0$ system. However, when $\eta \neq 0$, $Q_1 \neq 0$ and the analysis presented in Section 2 where linear terms dominate the behavior applies. The line of homoclinic

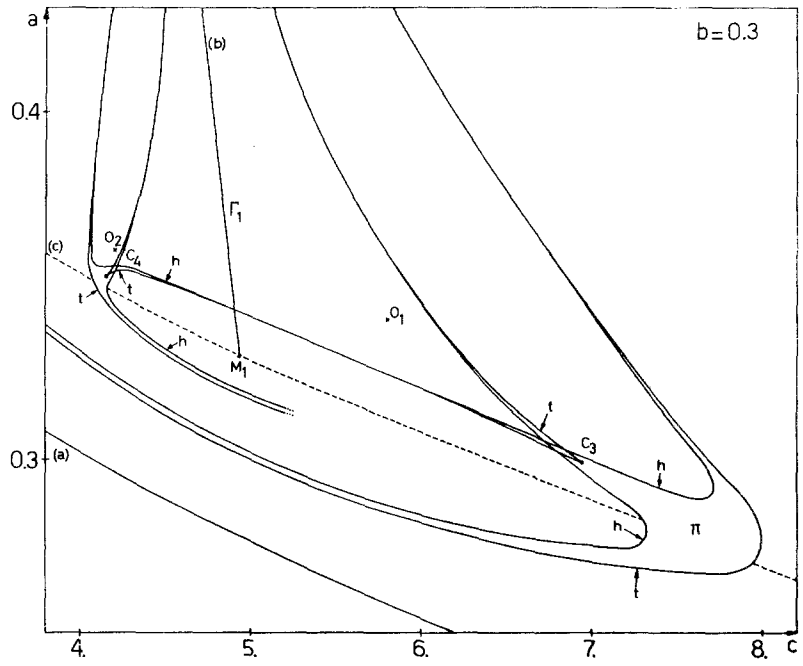

Fig. 5. Two-parameter (a, c) state diagram of the periodic attractors in the Rössler model (4.12). π: periodic attractor existence domain. Curve (a): accumulation line of the period-doubling sequence occurring below (a). Curve (b): set of systems containing a homoclinic orbit Γ_1 associated with the saddle-focus $(0, 0, 0)$. Curve (c): transition line between "spiral"- and "screw"-type chaos associated with homoclinic orbit Γ_1. M_1: end point of the line (b). c_3, c_4: two successive cusp bifurcation points. t: tangent bifurcation boundary of π. h: period-doubling bifurcation boundary of π.

systems is a parabola when $\eta \neq 0$ whose curvature depends on η. Very near to the set of homoclinic systems the envelope or tangent boundary is closely parallel to the parabola and does not contain a cusp point on such a fine scale. Thus, in a flow cusp bifurcations are expected only on a large scale and in finite number. However, the infinite contraction limit is a theoretical idealization which allows one to understand bifurcation phenomena near the onset of homoclinic behavior, in particular the cusp bifurcations which were studied in Ref. 12 for the following Rössler model[16]:

$$\begin{aligned} \dot{x} &= -y - z \\ \dot{y} &= x + ay \\ \dot{z} &= bx - cz + xz \end{aligned} \tag{4.13}$$

Earlier work[6] has established the location of the line of homoclinic systems Γ_1 in a two-parameter phase diagram for this system. The results of the present study suggest that the line Γ_1 acts as an organizing feature for the periodic orbit structure and their associated cusp bistabilities. That this is indeed the case is confirmed by the results in Fig. 5. This figure extends the results presented in Ref. 12 and shows that the period -3 cusp to the right of Γ_1 is continuously connected to a cusp bistability to the left of Γ_1. This figure should be compared with Fig. 4 as well as with Fig. 10 of the following section, which analyzes a class of one-dimensional maps.

5. ONE-DIMENSIONAL MAP MODEL

Many of the above mentioned aspects of the periodic orbit structure near homoclinic systems in the flow admit a simple description in terms of a class of two-parameter, multi-extremum, one-dimensional maps. One-dimensional-map models are most appropriate for the study of strongly dissipative systems: Eqs. (1.1) describe such systems provided the contraction of the flow along the stable manifold is much greater than the expansion along the unstable manifold; i.e., $|\lambda| \gg |\rho|$ and consequently $|\rho/\lambda| < 1/2$. Thus one might expect that many of the features of the bifurcation structure discussed in Section 4, which were deduced under the same conditions, are amenable to study by a one-dimensional map.

Consider the next-amplitude maps derived from Poincaré surfaces of section transverse to the two-dimensional unstable manifold of the flow (cf. Figs. 6 and 7a). A distinctive feature that typifies such maps of the flow near homoclinic orbits is the return of iterates to the vicinity of the unstable fixed point. The orbits of the map mimic the behavior of the trajectories of the flow: points near the unstable fixed point are mapped away from it in small steps corresponding to the winding motion of the flow trajectories on the unstable manifold of the saddle focus; the existence of a nearby

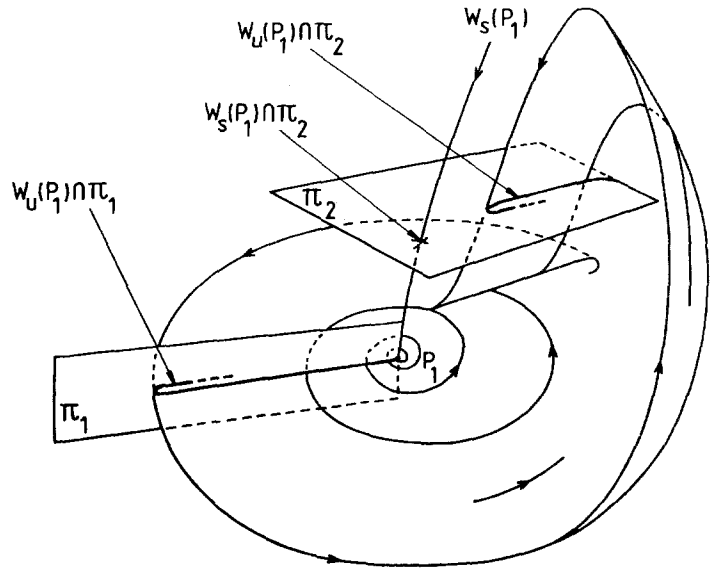

Fig. 6. Schematic representation of the flow on the Rössler (spiral) strange attractor. The unstable manifold $W_u(P_1)$ winds around the unstable fixed point P_1 and is reinjected onto the attractor disk near P_1; $W_s(P_1)$ is the stable manifold of P_1. The intersections of these manifolds with the plane π_2, $W_u(P_1) \cap \pi_2$ and $W_s(P_1) \cap \pi_2$ are a folded line and a point, respectively. π_1 is a surface-of-section plane transverse to the unstable manifold. The intersection of $W_u(P_1)$ with this plane, $W_u(P_1) \cap \pi_1$, is also shown. For the construction of the next amplitude maps in Fig. 7, π_1 was selected to be π_1: $y = 0$, $x < 0$.

homoclinic system ensures that the orbits of the flow and thus those of the map are returned to the neighborhood of the unstable fixed point. The important features of such maps are: the linear region, with slope $s = \exp(2\pi\rho/\omega)$ determined by the flow winding motion; the (typically rather broad) quadratic maximum arising from the smooth principal folding of the flow into itself (Fig. 6); and a minimum region which accounts for the reinjection of the flow trajectories into the vicinity of the unstable fixed point as the screw chaos line is crossed. A map with these general features is sketched in Fig. 8. As indicated in the figure two parameters can be used to control the dynamical processes of interest: ϵ which measures the height of the minimum and thus directly controls the reinjection process, as $\epsilon \to 0$ map iterates return to the origin; and the location of the map minimum, $m = 1 - \delta$, which determines the extent of the penetration of the system in the screw chaos region. If $\delta < 0$ the minimum disappears from the one-dimensional map. Thus, in the (ϵ, δ) plane the half-line $\epsilon = 0$, $\delta > 0$ corresponds to the line of homoclinic systems Γ of the

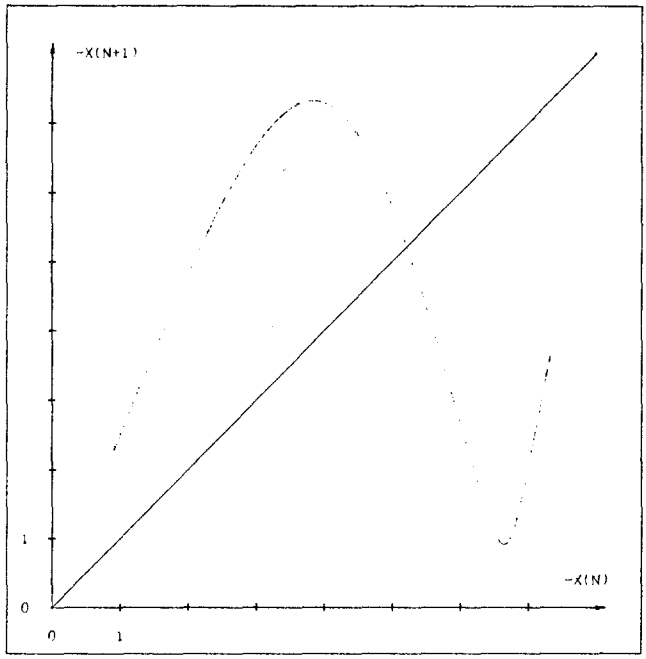

(a)

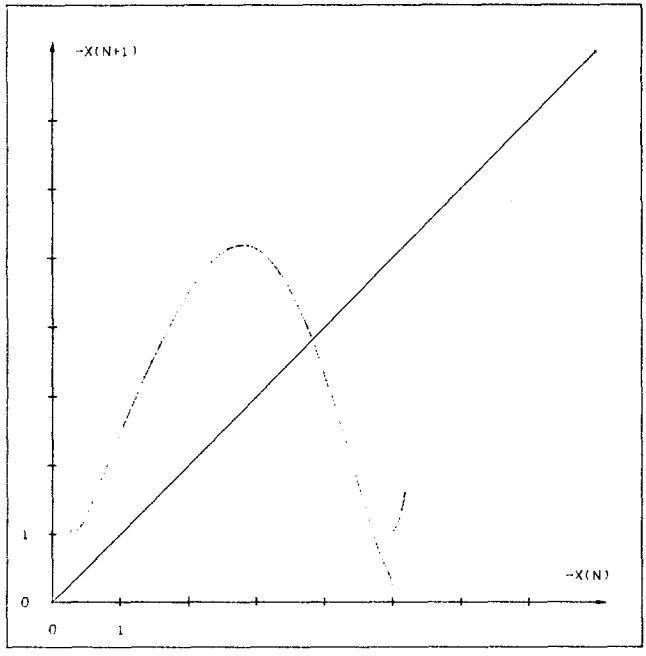

(b)

Fig. 7. (a) Next amplitude map for the Rössler screw strange attractor for $a = 0.34$, $b = 0.3$, and $c = 5.8$, point 0_1 in Fig. 5. (b) Same as (a) for $a = 0.36$, $b = 0.3$, and $c = 4.2$, point 0_2 in Fig. 5.

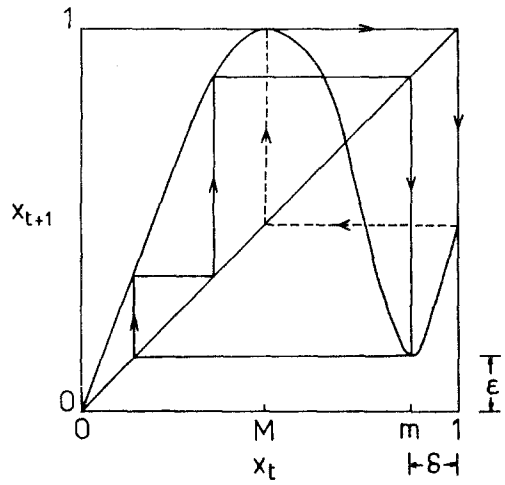

Fig. 8. A typical next amplitude map of the flow in the vicinity of a homoclinic system exhibiting a linear region near the origin, a broad quadratic maximum M and a sharper minimum m. The bifurcation parameters ϵ and δ are indicated. Also shown are coexisting superstable period-2 and period-3 orbits.

flow and the line $\delta = 0$ corresponds to the screw chaos line Σ. The map parameters ϵ and δ are not identical to those introduced in Section 4 but play similar roles.

In order to illustrate the properties of such a map model of the flow in a concrete fashion we consider a specific map with these features, but the qualitative aspects of our results are general. Referring again to Fig. 8 we parameterize the three relevant regions of the map in the following way:

$$f(x) = \begin{cases} f_l(x) = sx, & \text{linear region} \\ f_M(x) = 1 - c_M(x - M)^2, & \text{maximum region} \\ f_m(x) = \left[s_m^2(x - m)^2 + \epsilon^2 \right]^{1/2}, & \text{minimum region} \end{cases} \tag{5.1}$$

The specific form of the map in the minimum region reflects the observed sharpening of map minimum as the homoclinic system is approached (cf. Fig. 7a).[4] We focus on the sequence of stable period-n orbits ($n = 2, 3, 4, \ldots$) that consist of $n - 2$ iterates on the linear map and one iterate in

[4] The precise form of $f_m(x)$ fails to reflect one feature of the next-amplitude maps derived from the flow: from a consideration of the reinjection process one may argue that the ratio of the slope to the right of m to that to the left of m for $\epsilon = 0$ is $\exp(\pi\rho/\omega)$. The expression for $f_m(x)$ in Eq. (5.1) is symmetric with respect to m. While some quantitative aspects may be influenced by our form of f_m, the properties described below are independent of this choice.

each of the maximum and minimum regions. The structure of this sequence in the (ϵ, δ) plane is most conveniently characterized by examining the superstable orbits, i.e., those period-n orbits where one of the iterates lies exactly at a map extremum. Each extremum in the map can spawn a separate family of superstable orbits. This feature was previously noted in a cubic map model of the Rössler flow in the period-3 region where the particular configuration of the superstable lines was shown to give rise to the hysteresis and bistability.[12] The results presented below show that the two-extremum map of Eq. (5.1) duplicates the local features of the bifurcation structure discussed in the Sections 3 and 4.

The two families of superstable lines are constructed by requiring that the minimum or maximum belongs to the orbit: for a period-n orbit the slope of the nth composition of the map is zero and the orbit has maximum stability. The family of superstable orbits spawned by the minimum is determined by the equation,

$$f^{(n)}(m) = f_M\left(f_l^{(n-2)}(f_m(m))\right) = 1 - c_M(s^{n-2}\epsilon - M)^2 = m = 1 - \delta \quad (5.2)$$

and thus

$$\delta = c_M s^{2n-4}(\epsilon - Ms^{-n+2})^2 \quad (5.3)$$

If c_M and M are assumed independent of δ and ϵ the minimum superstable lines are locally parabolas centered at Ms^{-n+2} with curvature $2c_M s^{2n-4}$. The above analysis applies only for small δ and ϵ where the orbits have the assumed structure; the crossing of the superstable lines of members of this family when δ becomes large signals a breakdown of the approximation since two orbits with different period cannot have the fixed point m in common. The noncrossing constraint implies that the slopes of these lines must increase more strongly as δ increases than is predicted by (5.3), but a complete specification of the map is necessary to fix this detail. If we consider δ fixed at a large positive value the sequence of ϵ values corresponding to superstable orbits is given by

$$\epsilon_n = \left[M \pm \left(\frac{\delta}{c_M}\right)^{1/2}\right] s^{2-n} \sim s^{-n} = \exp\left(-2\pi \frac{\rho}{\omega} n\right) \quad (5.4)$$

in accord with Eq. (3.8). The superstable lines associated with the maximum follow from the condition that M is a fixed point of period n:

$$M = f_l^{(n-2)}(f_m(f_M(M))) = s^{n-2}\left[(s_m\delta)^2 + \epsilon^2\right]^{1/2} \quad (5.5)$$

or

$$\epsilon^2 + (s_m\delta)^2 = (Ms^{2-n})^2 \quad (5.6)$$

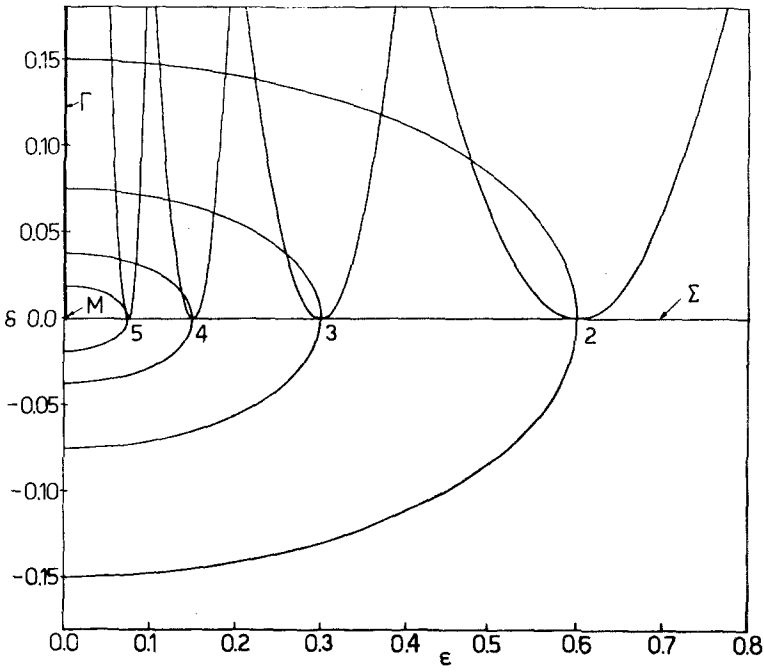

Fig. 9. Superstable lines for periods 2, 3, 4, and 5 associated with the maximum and minimum of the map. The lower crossing points on the $\delta = 0$ screw chaos line Σ correspond to doubly superstable orbits, while the upper crossing points correspond to coexisting superstable orbits. The map parameters used in the construction of this figure are: $s = 2$, $M = 0.6$, $s_m = 4$, and $c_M = 6$.

The configuration of the maximum and minimum superstable lines is displayed in Fig. 9, which illustrates a number of features associated with this sequence of orbits. In accord with Eq. (5.4) the family of superstable orbits spawned by the minimum accumulates at the line of homoclinic systems Γ, while the family of superstable orbits associated with the maximum accumulates at the point M, which is the end point of the line of homoclinic systems. The scaling of this latter family along the line $\epsilon = 0$ easily follows from Eqs. (5.6):

$$\delta_n = \pm \frac{M}{s_m} s^{2-n} \sim \exp\left(-2\pi \frac{\rho}{\omega} n\right) \tag{5.7}$$

Furthermore, the superstable lines for each member of the sequence of period-n orbits cross twice. By construction of the map, the lower crossings, which always lie on the screw chaos line Σ, correspond to doubly superstable-

ble orbits where both the maximum and minimum belong to the orbit. Thus, the point M is also the accumulation point of the doubly superstable orbits. While the lower crossings of the superstable lines along Σ correspond to doubly superstable orbits, the upper crossings are related to bistability where two distinct superstable orbits with period-n coexist; these upper crossing points also accumulate at M. This (local) bistability between period-n orbits of the sequence should be distinguished from the bistability that arises from the crossing of the superstable lines associated with different members sequence (cf. Fig. 9). (As an illustration of this latter type of bistability coexisting superstable period-3 and period-2 orbits are shown in Fig. 8.) We discuss the local bistability in more detail below. The structure in Fig. 9 thus implies a complex web of bistabilities in the vicinity of Γ: orbits of the minimum sequence with high periods coexist with members of the maximum sequence with increasing periods as M is approached. Such bistability can only exist above Σ since below this line the map possesses a single extremum and the family spawned by the minimum cannot exist.

We next construct the tangent and harmonic boundaries which determine the limits of stability of the period-n orbits. This will allow us to relate the boundary structure in the one-dimensional map directly to the analogous structure described in Section 4.

These boundaries may be determined easily from the solutions of the simultaneous equations,

$$f^{(n)}(x) - x = 0 \quad \text{and} \quad f^{(n)'}(x) = \begin{cases} +1 & \text{tangent} \\ -1 & \text{harmonic} \end{cases} \tag{5.8}$$

For the map of Eq. (5.1) we find

$$s^{n-2}\left\{ s_m^2\left[\delta - c_M u^2 \right]^2 + \epsilon^2 \right\}^{1/2} - u = M \tag{5.9}$$

and

$$u^3 - \left(\frac{\delta}{c_M} \pm \alpha_n^{-1} \right) u \mp M\alpha_n^{-1} = 0 \tag{5.10}$$

where $u = x - M$ and $\alpha_n = 2s^{2n-4}s_m^2 c_M^2$. The upper signs again refer to tangent boundaries and the lower signs to harmonic boundaries. We first note that for $\epsilon = 0$, i.e., along the line of homoclinic systems, these equations are easily solved to yield

$$\delta_n^{t,h} = \frac{M}{s^{n-2}s_m} + \begin{Bmatrix} -1 \\ +3 \end{Bmatrix} \left(4c_M s_m^2 s^{2n-4} \right)^{-1} \tag{5.11}$$

Hence on Γ there exists a sequence of stable periodic orbits accumulating

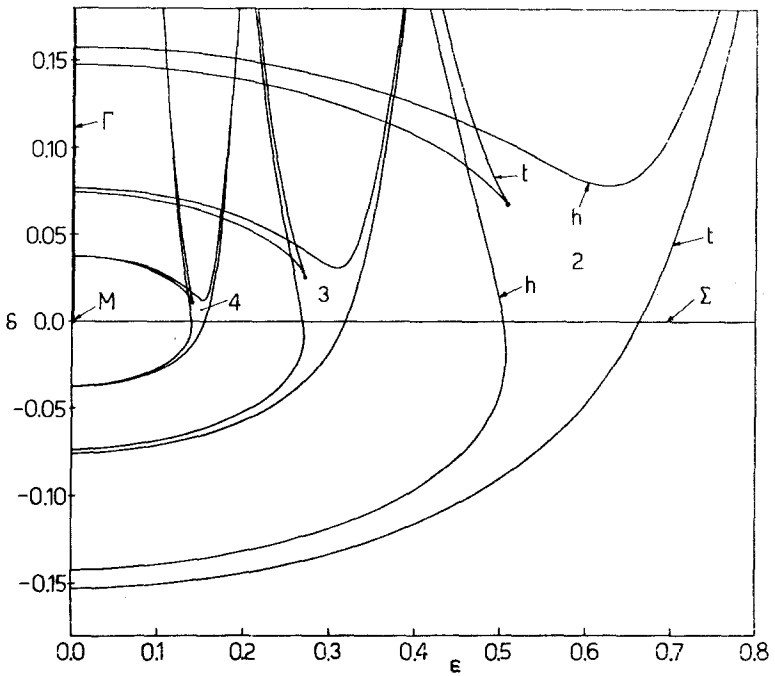

Fig. 10. Tangent t and harmonic h boundaries in the (ϵ, δ) plane for periods 2, 3, and 4. A cusp structure similar to that of Section 3 is clearly evident. The map parameters are the same as for Fig. 9.

at M whose windows of stability have width

$$\delta_n^h - \delta_n^t = \left(c_M s_m^2 s^{2n-4}\right)^{-1} \sim \exp\left(-4\pi \frac{\rho}{\omega} n\right) \tag{5.12}$$

The boundaries are sketched in Fig. 10, which shows that each member of the sequence possesses a cusp structure similar to that found in Section 3. The characteristic configuration for a period-n orbit consists of an outer tangent boundary t where the orbit is born by a tangent bifurcation; the inner crossing harmonic boundaries h signal the subharmonic bifurcation of period n to period $2n$. Within the cusp shaped tangent boundary t bistability between a period-n orbit and its coexisting mate and its subharmonics is observed. The dynamics in such a region has been described in some detail earlier for related one-dimensional maps.[12]

The analysis of the flow in Sections 3 and 4 has demonstrated that the period-n orbits in the sequence are connected in a spiral structure—the orbits can be continuously deformed into one another by tuning the two bifurcation parameters. This feature is outside the scope of the one-

dimensional map of Eq. (5.1), which is capable of describing the behavior for $\epsilon > 0$ only. The restriction arises from the selection of the surface of section used to construct the next-amplitude map. Figure 6 illustrates this point for the Rössler flow. Using the π_1 plane for the surface of section, map parameter $\epsilon > 0$ corresponds to the situation where the flow is reinjected onto the attractor disk near the unstable fixed point to the right of the stable manifold. If one continuously tunes the flow parameters to the region left of Γ_1 the flow is now reinjected on the left side of the stable manifold and the corresponding next amplitude map possesses a discontinuity (cf. Fig. 7b). Such artifacts in the map can be removed by selecting a new surface-of-section plane. Thus, a full description of the orbit structure in terms of the one-dimensional map also entails the choice of the appropriate section plane as the flow parameters are tuned. We shall not pursue this aspect further here but instead briefly comment on a related phenomenon near homoclinicity, which is suggested by the one-dimensional map.

We have calculated and described the harmonic boundaries where a period-n orbit born by a tangent process bifurcates to yield an orbit with period $2n$. For a map with the structure in Fig. 8 there exists a cascade of such subharmonic bifurcations yielding orbits with period $n\,2^k$, which exhibits a number of interesting features. In particular, for such two-parameter, two-extremum maps there exists an infinite hierarchy (Cantor set) of cusp bistabilities for each member of the sequence of period-n orbits. The mechanism of the origin and scaling properties of this cusp hierarchy have been described in some detail for the sine map.[17] Since the primary period-n orbits are all continuously connected on the spiral structure, the cusp hierarchy arising from the subharmonic bifurcations will also form part of this connected structure. The discussion of this section suggests that such cusp hierarchies should be a common feature of flows near homoclinic systems.

6. DISCUSSION

The two-parameter analysis performed in this paper has revealed a remarkable bifurcation structure in the vicinity of Sil'nikov's homoclinic systems: a countable number of stable periodic solutions; period-doubling transitions from these orbits, which potentially can lead to chaotic attractors via Feigenbaum cascades; and cusp bifurcations, with concomitant bistability and hysteresis. Thanks to the latter, different periodic orbits are continuously connected in the parameter space. Moreover, their stability windows are enlarged near the cusp singularities.

We have established the existence of scaling properties of the sequence of periodic solutions in the parameter space, which are determined entirely

by the parameters ρ and ω of the underlying flow. Two properties which at first appear to be independent are thus linked near homoclinicity: a *global* feature like the bifurcation of the periodic attractors, and a *local* one like the characteristics of the time evolution of the system near the stationary state.

We believe that our results illustrate the importance of homoclinic orbits as an organizing principle of the bifurcations leading to complex nonperiodic behavior in large classes of dynamical systems. Furthermore, they provide a plausible interpretation of a number of experimental results in which alternating periodic and chaotic sequences are observed. For instance, the Belousov–Zhabotinski reaction[18–20] a regular sequence of period-n regimes with increasing periods is interrupted by chaotic regions, as the bifurcation parameter is varied. Characteristically, the chaotic state lying between period-n and period-$(n+1)$ orbits is the chaotic mixture of these neighboring periodic orbits. The experiments also show that a period-n orbit may lose its stability and become chaotic via a period-doubling cascade, whereas the period-$(n+1)$ orbit is born by a tangent bifurcation.[21] Similar sequences have been observed in electronic switching circuits.[22] All this is strongly reminiscent of the behavior depicted in Fig. 3.

Needless to say, the problem of bifurcations in near homoclinic systems is far from solved. One obvious extension of our analysis is to systems of four or more variables. Some results in this area are already available[10] but so far the bifurcation structure has not been revealed in a satisfactory way. Another direction is toward a deeper understanding of the effect of the complex transitions going on near a homoclinic system on the ergodic properties of the flow. Moreover, it would be interesting to see whether homoclinic orbits and their bifurcations can lead to a better understanding of certain transition phenomena observed in physicochemical systems in which a fixed point of the saddle-focus type is generated through the coupling between an oscillatory and a monotonic mode.

ACKNOWLEDGMENTS

R. Kapral thanks Professor Prigogine for his hospitality during the author's stay in Brussels. This research was carried out during the tenure of a fellowship of the Institut pour l'Encouragement de la Recherche Scientifique dans l'Industrie et l'Agriculture by P. Gaspard. It is supported in part, by the U.S. Department of Energy under Contract No. DE-AS05-81ER10947 and by the Natural Sciences and Engineering Research Council of Canada.

REFERENCES

1. J. Guckenheimer, Dynamical systems, *Progress in Mathematics*, Vol. 8 (Birkhaüser, Basel, 1980).
2. S. Smale, *Bull. Am. Math. Soc.* **73**:747 (1967).
3. M. J. Feigenbaum, *J. Stat. Phys.* **19**:25 (1978); **21**:669 (1979).
4. A. Arneodo, P. Coullet, and C. Tresser, *J. Stat. Phys.* **27**:171 (1982).
5. C. Sparrow, *The Lorenz Equations: Bifurcation, Chaos and Strange Attractors* (Springer, New York, 1982).
6. P. Gaspard and G. Nicolis, *J. Stat. Phys.* **31**:499 (1983).
7. P. Gaspard, Generation of a countable set of homoclinic flows through bifurcation, *Phys. Lett.* **97A**:1 (1983).
8. P. Gaspard, Mémoire de Licence, University of Brussels, 1982.
9. A. Andronov, E. Leontovitch, I. Gordon, and A. Maier, *Theory of Bifurcation of Dynamic Systems on a Plane* (Israel program of scientific translations, Jerusalem, 1971).
10. J. Neimark and L. Sil'nikov, *Sov. Math. Dokl.* **6**:305 (1965); L. Sil'nikov, *Sov. Math. Dokl.* **6**:163 (1965); *Math. Sbornik.* **10**:91 (1970); *Sov. Math. Dokl.* **8**:54 (1967).
11. V. Afraimovitch, V. Bykov, and L. Sil'nikov, *Sov. Phys. Dokl.* **22**:253 (1977).
12. S. Fraser and R. Kapral, *Phys. Rev. A* **25**:3223 (1982).
13. P. Glendinning and C. Sparrow, Local and global behavior near homoclinic orbits, preprint.
14. P. Hartman, *Ordinary Differential Equations* (Wiley, New York, 1964).
15. H. Whitney, *Ann. Math.* **62**:374 (1955).
16. O. Rössler, *Ann. N.Y. Acad. Sci.* **316**:376 (1979).
17. M. Schell, S. Fraser, and R. Kapral, *Phys. Rev. A* **28**:373 (1983).
18. J. L. Hudson, M. Hart, and D. Marinko, *J. Chem. Phys.* **71**:1601 (1979).
19. J. S. Turner, J.-C. Roux, W. D. McCormick, and H. L. Swinney, *Phys. Lett.* **85A**:9 (1981).
20. C. Vidal, in *Chaos and Order in Nature*, H. Haken, ed. (Springer, Berlin, 1981), p. 69.
21. J.-C. Roux and H. L. Swinney, in *Nonlinear Phenomena in Chemical Dynamics*, A. Pacault and C. Vidal, eds. (Springer, Berlin, 1981).
22. A. S. Pikovsky and M. I. Rabinovich, *Physica* **20**:8 (1981).